RESEARCH ARTICLE

Particle & Particle Systems Characterization
www.particle-journal.com

Seed-Mediated Synthesis of Gold Nanobipyramids at Low CTAB Concentration Using Binary Surfactants

Er-Ji Zhang, Tian-Song Deng, Zhuo Chen, Li-Yong Liu, Gui-Lin Wu, Yu-Chun Cheng, Jia-Fei Gao, Kun-Peng Wang, and Jie Liu*

The conventional method for synthesizing gold nanobipyramids (AuNBPs) is well established. However, the cytotoxicity resulting from the conjugates between hexadecyltrimethylammonium bromide (CTAB) and gold limits their biomedical applications. This study introduces a dual surfactant approach with CTAB and sodium oleate (NaOL) in the seed-mediated synthesis of the AuNBPs, which can significantly reduce the CTAB concentration to 10 mM. Additionally, optimal growth conditions are achieved by varying the volumes of seed solution, $AgNO_3$, and HCl. Under low CTAB concentrations, AuNBPs with tunable sizes and localized surface plasmon resonances between 600 and 1200 nm are successfully synthesized, as characterized by UV–vis-NIR spectroscopy, transmission electron microscopy (TEM), and finite-difference time-domain (FDTD) simulations. This work demonstrates a method for synthesizing AuNBPs at low CTAB concentrations using binary surfactants and provides a framework applicable to the synthesis of other metallic nanomaterials.

1. Introduction

Noble metal nanoparticles exhibit unique properties distinct from bulk noble metal materials, such as gold and silver, in structures like nanorods and nanospheres.[1] They demonstrate excellent performances in light absorption and scattering. When incident light matches the frequency of the collective oscillation of electrons (plasmon resonance) within these metallic nanoparticles, strong absorption of photon energy occurs, resulting in a prominent resonance peak in the spectrum. This phenomenon is known as localized surface plasmon resonance (LSPR).[2] The localized plasmon modes of gold and silver nanostructures offer highly tunable properties across a broad spectral range from visible to near-infrared light. This tunability underpins their wide-ranging potential applications in catalysis,[3,4] solar energy harvesting,[5,6] surface-enhanced spectroscopy,[7,8] and biomedical fields.[9,10]

AuNBPs[11–13] and gold nanorods (AuNRs)[14,15] are two typical types of elongated gold nanocrystals that exhibit tunable longitudinal plasmon resonance wavelengths spanning from visible to near-infrared regions. Similar to AuNRs, the LSPR of AuNBPs also includes transverse and longitudinal modes, with the latter directly determined by the dimensions of the nanobipyramids. This feature allows for tailored plasmonic properties through specific synthesis approaches. In contrast to AuNRs, which typically have an octagonal cross-section and flat or chamfered ends, AuNBPs consist of two cones with pentagonal bases joined at their bottoms and oriented along their axes with five equally spaced growth facets. Consequently, AuNBPs have two sharp tips, while AuNRs have circular or flattened ends, resulting in significantly different plasmonic characteristics between the two nanoparticles.

Generally, compared to AuNRs, AuNBPs exhibit larger and more concentrated local electric field enhancements. This allows us to have greater potential in utilizing their plasmonic enhancement capabilities. Moreover, the synthesized AuNBPs often demonstrate higher monodispersity and narrower LSPR bandwidths,[16] which avoids spectral broadening caused by product non-uniformity, theoretically making them superior candidates for sensing applications. Despite these attractive features, the quantity and purity of colloidal AuNBPs samples are typically lower than those of AuNRs, which further limits their practical application space, despite their unique characteristics.

The synthesis method of AuNBPs is similar to that of AuNRs, typically prepared using the seed-mediated growth method commonly employed in nanoparticle synthesis.[17,18] This method generally involves two steps: seed preparation and subsequent seed growth. In seed-mediated growth, the quality of the seeds and growth conditions significantly influence the final quality of the synthesized AuNBPs. Only seeds with pentatwinned structures will eventually grow into AuNBPs. Therefore, the proportion of pentatwinned seeds in the seed solution determines the yield of AuNBPs.

Initially, the synthesis of high-purity pentatwinned seeds was not well developed, resulting in a yield of only ≈30% for AuNBPs.[19] To obtain high-purity AuNBPs, multiple tedious purification methods are necessary to separate them from spherical and irregular polyhedral impurities, significantly increasing the experimental difficulty. Subsequently, the Liz-Marzán group addressed the purity issue in synthesizing AuNBPs by heat treatment of the seeds. After the heat treatment, the proportion of

E.-J. Zhang, T.-S. Deng, Z. Chen, L.-Y. Liu, G.-L. Wu, Y.-C. Cheng, J.-F. Gao, K.-P. Wang, J. Liu
School of Electronics and Information Engineering
Hangzhou Dianzi University
Hangzhou 310018, P. R. China
E-mail: dengts@pku.edu.cn

The ORCID identification number(s) for the author(s) of this article can be found under https://doi.org/10.1002/ppsc.202400190

DOI: 10.1002/ppsc.202400190

pentatwinned structures in the seed solution significantly increased, and the yield of AuNBPs also improved to ≈90%.[18] Liang et al. achieved high yield and reproducible production of small-sized gold nanodecahedrons (AuNDs) nanocrystals, and further used them as seeds to controllably synthesize monodisperse AuNBPs and other shaped nanocrystals.[20] This method of preparing AuNBPs exhibits better photothermal conversion properties compared to other shapes of gold nanocrystals.

However, seed quality is not the only factor influencing the synthesis of the AuNBPs. Conditions such as surfactants,[21] pH,[22] and other factors in the growth solution also affect the types and purity of the gold nanoparticles synthesized. In different growth solutions, even with the same pentatwinned seeds, different shapes of nanoparticles could be produced.[12] This underscores the importance of studying growth conditions for precise control over the size and plasmonic properties of the AuNBPs.

The synthesis of AuNBPs typically occurs in aqueous solutions containing CTAB, $HAuCl_4$, $AgNO_3$, HCl, and ascorbic acid (AA). The primary reaction in experiments usually involves the reduction of Au(III) ions to Au(0) atoms by AA, which gradually deposits onto the seed surface, facilitating growth into the final product. Surfactants (CTAB) and Ag(I) ions are also essential in the synthesis. Ag acts as a specific surface structure surfactant, depositing in a monolayer form as Ag(0) due to its underpotential deposition from Ag(I). Surfactant (CTAB) acts as stabilizers and structure-directing agents based on their binding energy dependence on crystal facets; larger surfactant headgroups generally yield higher yields of AuNBPs. Other reaction conditions affecting crystal growth, such as pH, have been minimally studied, its influence primarily regulates reaction rates and does not decisively affect outcomes. Researchers have attempted various improvements to control the types and purity of synthesized nanoparticles.

For instance, Zhang et al. achieved different types of pentatwinned nanocrystals (spheres, bipyramids, and decahedrons) in the same high-purity system by altering the initial pH of the growth solution.[22] Li et al. demonstrated the production of various types of high-purity, size-tunable pentatwinned nanocrystals (truncated bipyramids, truncated ditetrahedrons, ditetrahedrons, truncated twinned ditetrahedrons, star-shaped pentatwinned nanocrystals, concave tetrahedrons, and tetrahedrons) in a single system solely by adjusting the deposition kinetics of attached atoms at different positions on decahedral seeds.[23] Zhong et al. propose a strain modulation strategy to produce branched Au nanostructures that promote the growth of Au on Au seeds in the Volmer–Weber mode.[24] The key to this strategy is to continuously deposit polydopamine formed in situ on the growing surface of the seeds to increase the chemical potential of the subsequent deposition of Au, thus achieving continuous heterogeneous nucleation and growth. Chen et al. explore the use of spherical shape-deformable polymeric nanoshells to regulate the anisotropic growth of Ag nanoplates.[25] The flexible shells deform adaptively to accommodate the initial overgrowth of the seeds eventually producing nanoplates with an unconventional circular profile.

However, in existing methods for synthesizing AuNBPs, the majority utilize high concentrations of CTAB (0.1 M) as the surfactant. It's crucial to note that the toxicity of CTAB bound to gold nanoparticles can cause significant damage to biological cells and tissues, thereby impacting the biomedical applications of these nanoparticles. According to experiments conducted by Ray et al.,[26] under the influence of AuNRs@CTAB, only a small percentage of cells (≈10%) survive. Furthermore, they noted that varying sizes of gold nanoparticles coated with citrate salts were non-toxic to human skin cells, but due to CTAB as the coating material, AuNRs@CTAB exhibited severe toxicity. Lau et al.[27] studied the in vitro apoptotic induction of human red blood cells by CTAB and PEG-modified AuNRs, demonstrating that CTAB-modified AuNRs exhibited cellular toxicity, whereas PEG-modified AuNRs did not. The toxicity of CTAB-modified AuNRs is primarily attributed to residual CTAB from incomplete purification of AuNRs or desorption of CTAB bilayers bound to the nanoparticles. Rajeshwari et al.[28] assessed the cytogenetic effects of CTAB and PEG-modified AuNRs on plant cells using bioassays, and found that both types induced toxicity in the plant system after 4 h of interaction, with CTAB-modified AuNRs causing a reduction in mitotic index 40 times higher than that induced by PEG-modified ones at a maximum concentration of $10\ \mu g\ mL^{-1}$. Based on these findings, researchers have attempted to mitigate the toxicity of CTAB-modified AuNRs by attempting to remove the CTAB surface modification.[29,30] However, removing CTAB renders the AuNRs unstable in aqueous dispersion. While this significantly reduces their toxicity, it also renders them unsuitable for studying their physicochemical properties in solution.

In this study, we report the synthesis of AuNBPs using a binary surfactant system (CTAB and NaOL) with a significantly lower concentration of CTAB (as low as 10 mM, ≈10% of that used in previous works) via a seed-mediated growth method. Additionally, the concentration of NaOL was only 2 mM, while the synthesized AuNBPs maintained high monodispersity. We further investigated the effects of seed solution, $AgNO_3$, and pH on the synthesis of AuNBPs and optimized the growth conditions under low CTAB concentration (10 mM). The synthesized AuNBPs were characterized using UV–vis-NIR spectroscopy and TEM. Based on the dimensions obtained from TEM, we conducted FDTD simulations to calculate the full-field scattering spectra and electric field distribution of AuNBP nanostructures with different sizes. These simulations corroborated the accuracy of our experimental data.

2. Results and Discussion

We synthesized AuNBPs using a modified seed-mediated method in a growth solution containing binary surfactants CTAB and NaOL. The seed solution preparation followed the method published by Liz-Marzán in 2017.[18] Briefly, seeds were prepared by rapidly reducing $HAuCl_4$ with the strong reductant $NaBH_4$. The seeds were then aged at 80 °C for 90 min in the presence of sodium citrate and CTAC to obtain thermodynamically stable pentatwinned seeds. This method significantly increased the yield of AuNBPs to 90% without purification.

For the growth solution, we referred to the common formulations for AuNBP growth solutions and the dual-surfactant synthesis method for AuNRs published by Ye in 2013.[14] We made some modifications to the experiments. First, the prepared CTAB solution and NaOL solution were mixed (alternatively, they could

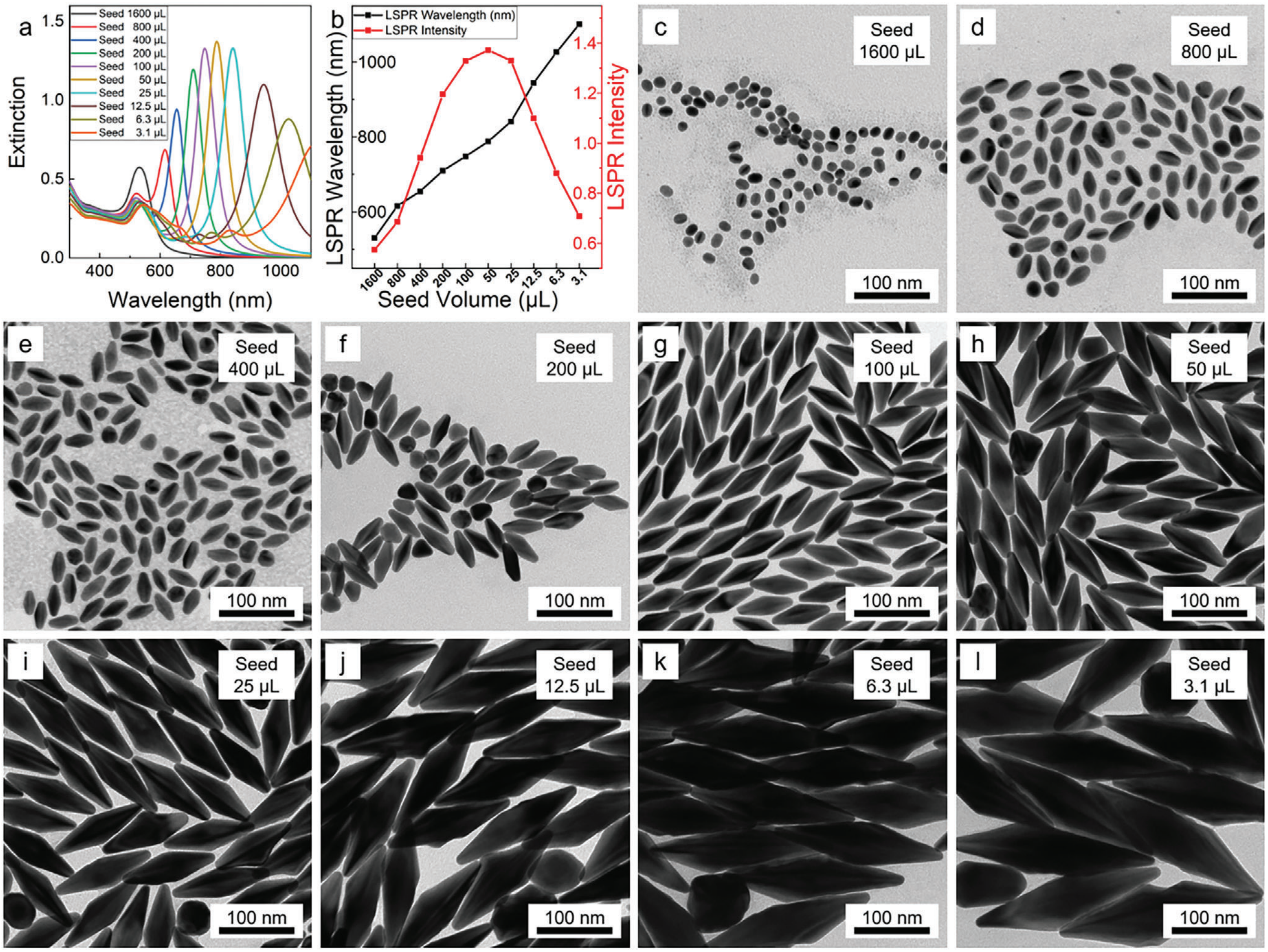

Figure 1. UV–vis-NIR spectra and TEM images of AuNBPs synthesized with different seed volumes. a,b) UV–vis-NIR spectra and corresponding LSPR peak positions and intensities of AuNBPs synthesized with different seed volumes. c–l) TEM images of AuNBPs synthesized with different seed volumes, with images from (c) to (l) corresponding to seed volumes ranging from 1600 to 3.1 µL.

be directly weighed and prepared for immediate use). $HAuCl_4$ solution was added to this mixture and stirred slowly at 30 °C. Due to the weak reducing property of NaOL, Au(III) was reduced to Au(I), causing the solution color to change from orange-yellow to colorless and transparent. Subsequently, $AgNO_3$, HCl, and AA were added to the solution in sequence. Finally, the seed solution was added. After slow stirring for 24 h, the AuNBPs were obtained. Detailed experimental procedures can be found in the experimental section.

Based on the above experiments, we further investigated the impact of all parameters on the synthesis of AuNBPs, including seed volume, Ag^+ concentration, and pH. According to previous studies,[12] the volume of the seed solution added is crucial in determining the size of the synthesized AuNBPs. As shown in **Figure 1**, we attempted to add different volumes of seed solution to the same growth solution, resulting in a series of AuNBPs of varying sizes. When a larger volume of seed solution was added, the synthesized AuNBPs particles were very small and, due to the limited amount of the gold precursor, did not exhibit a complete bipyramidal shape, appearing more ellipsoidal instead. As the volume of the seed solution decreased, the number of gold atoms each seed could acquire increased exponentially, leading to larger AuNBPs particles. The size of the particles ranged from ellipsoidal nanoparticles with a length of 18 nm and a width of 13 nm to giant nanoparticles with a length of 270 nm and a width of 65 nm.

We also plotted the relationship between the LSPR peak position and intensity against the volume of seed solution added, as shown in Figure 1b. As the volume of the seed solution decreased, the size of the AuNBPs particles increased, causing a red shift in the corresponding LSPR peak. The intensity of the LSPR peak first increased and then decreased, reaching its maximum when the volume of the seed solution was 50 µL. The resulting AuNBPs spectra could be tuned from 600 to over 1100 nm (Figure 1a). The detailed data of size and LSPR peak position for AuNBPs synthesized with different seed volumes can be found in Table S1 (Supporting Information).

Similarly, we investigated the effect of Ag^+ ion concentration on the synthesis of AuNBPs. As shown in **Figure 2**, we synthesized a series of AuNBPs by varying the amount of $AgNO_3$

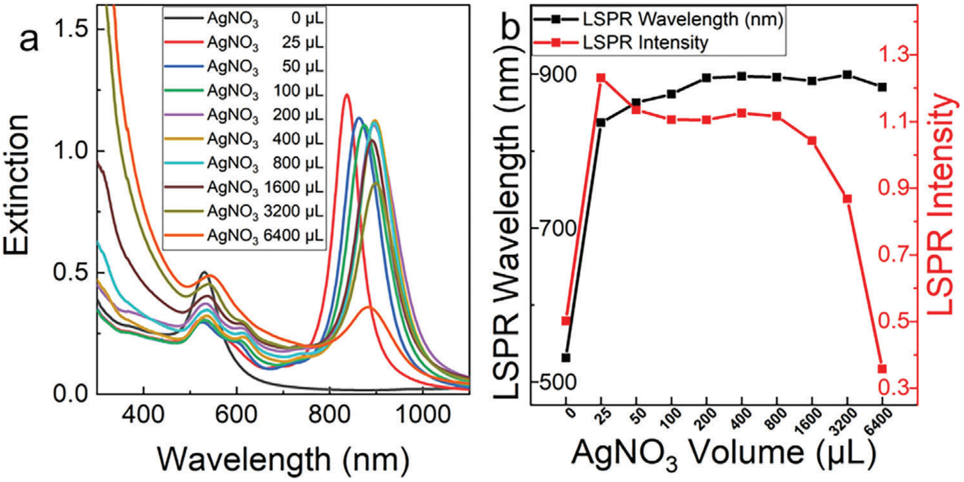

Figure 2. UV–vis-NIR spectra a) and corresponding LSPR peak positions and intensities b) of AuNBPs synthesized with different $AgNO_3$ volumes.

solution added and recorded the corresponding changes in the LSPR peak position and intensity. From Figure 2b, one can see that when no Ag^+ ions were introduced into the growth solution, the extinction spectrum exhibited only one absorption peak at 530 nm, indicating the absence of AuNBP structures. However, with the introduction of a small number of Ag^+ ions, two absorption peaks appeared in the extinction spectrum, and the LSPR peak underwent a red shift with increasing amounts of Ag^+ ions until the $AgNO_3$ solution volume reached 200 µL, at which point the redshift was maximized. Further increases in Ag^+ ion concentration resulted in a gradual decrease in the LSPR peak intensity, accompanied by the emergence of a new Ag-related absorption peak at 300 nm. Based on the above experiments, we determined that the appropriate range for adding $AgNO_3$ is between 25 and 100 µL. Detailed data of the LSPR peak position for AuNBPs synthesized with different $AgNO_3$ volumes can be found in Table S2 (Supporting Information).

Additionally, we observed the formation of a white flocculent precipitate with excessive Ag^+ ion introduction, which we identified as an AgCl precipitate. The amount of this precipitate increased with the Ag^+ ion concentration. Notably, the formation of AgCl precipitate was not exclusive to changes in Ag^+ ion concentration. Initially, our method involved introducing $HAuCl_4$ in the presence of CTAB, NaOL, and $AgNO_3$, with NaOL slowly reducing Au(III) to Au(I). However, when attempting to lower the CTAB concentration, an anomalous AgCl precipitate appeared only at a CTAB concentration of 10 mм. Slight increases or decreases in CTAB concentration did not lead to AgCl precipitate formation. To address this issue, we modified the reagent addition sequence in the experiment, delaying the introduction of $AgNO_3$ solution until after Au(III) had been pre-reduced to Au(I). This adjustment successfully prevented the formation of anomalous AgCl precipitate.

Subsequently, we studied the effect of pH on the synthesis of AuNBPs. As shown in **Figure 3**, we synthesized a series of AuNBPs by varying the volume of HCl solution added and recorded the corresponding changes in the LSPR peak position and intensity. Figure 3b demonstrates that when the volume of

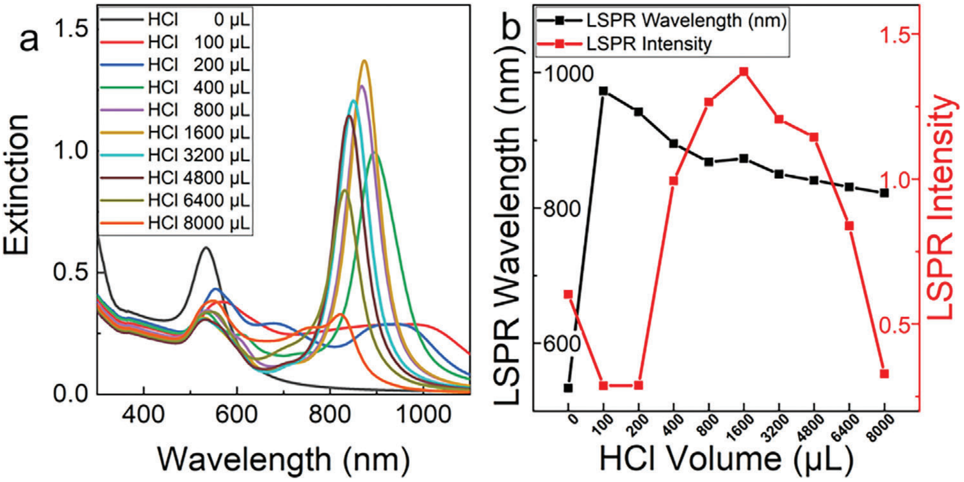

Figure 3. UV–vis-NIR spectra a) and corresponding LSPR peak positions and intensities b) of AuNBPs synthesized with different HCl volumes.

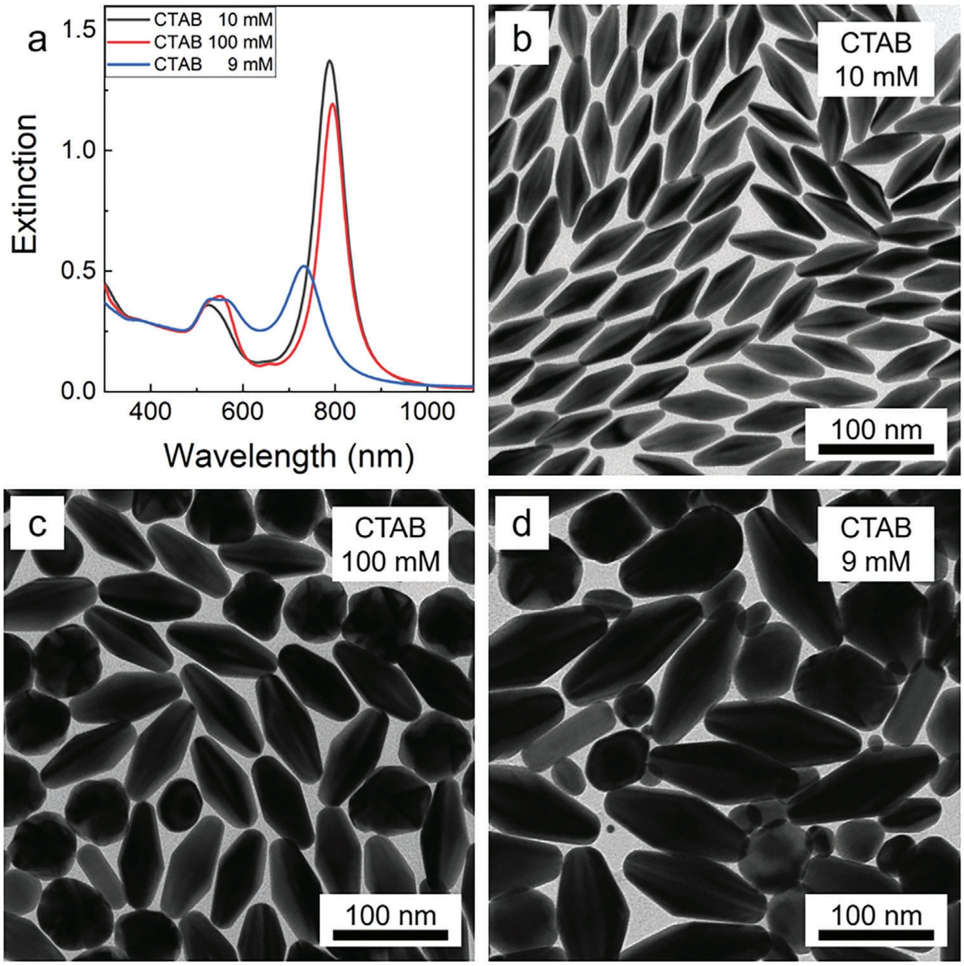

Figure 4. UV–vis-NIR spectra and TEM images of AuNBPs synthesized at different CTAB concentrations. a) UV–vis-NIR spectra of AuNBPs synthesized at different CTAB concentrations. b–d) TEM images of AuNBPs synthesized at CTAB concentrations of 10 mM (b), 100 mM (b), and 9 mM (d), respectively.

HCl added was small (0–200 µL), the extinction spectra did not exhibit a normal LSPR absorption peak, indicating the absence of AuNBPs in the solution. Conversely, when a larger volume of HCl was added (400–8000 µL), the extinction spectrum showed a strong LSPR absorption peak. As the volume of HCl increased, the LSPR peak position experienced a blue shift to some extent, and the intensity first increased and then decreased. Based on the above experiments, we determined that the appropriate range for adding HCl is between 800 and 3200 µL. Detailed data of the LSPR peak position for AuNBPs synthesized with different HCl volumes can be found in Table S3 (Supporting Information).

To understand the effect of HCl on the AuNBPs synthesis, it is essential to know that the reducing agent in the experiment, AA, provides its reducing power through the hydrolysis product, the ascorbate ion, rather than AA itself. The ionization equation of AA in aqueous solution is as follows:

$$C_6H_8O_6 \rightleftharpoons C_6H_7O_6^- + H^+ \tag{1}$$

The hydrolysis of AA in the solution is affected by the concentration of H^+ ions. When a small volume of HCl is added, the pH of the solution is relatively high, and the hydrolysis of AA is not significantly inhibited. This results in an excess production of ascorbate ions, leading to a very rapid reduction rate and the formation of an excessive number of gold atoms in a short period. This disrupts the selective deposition of gold atoms on the seed surface, preventing the formation of the desired bipyramidal structure.

In contrast, when a larger volume of HCl is added, the pH of the solution is lower, significantly inhibiting the hydrolysis of AA. Consequently, the concentration of ascorbate ions in the solution is limited, resulting in a slower reduction rate of gold atoms. This slower reduction allows the gold atoms more opportunity to selectively deposit on the sides of the seeds, ultimately growing into AuNBPs.

In the experiments, we also attempted to lower the concentrations of the surfactants CTAB and NaOL for synthesizing AuNBPs. As shown in **Figure 4**, UV–vis-NIR spectra and corresponding transmission electron microscopy (TEM) images of AuNBPs synthesized under different CTAB concentrations (10, 100, and 9 mM) using the dual-surfactant method are presented. In Figure 4a, the spectra are represented by black for CTAB concentration of 10 mM, red for 100 mM, and blue for 9 mM. We successfully reduced the CTAB concentration to 10 mM without altering the spectral intensity and peak positions of the synthesized AuNBPs.

In control experiments, we initially used a NaOL concentration of 8 mM and varied the CTAB concentrations to synthesize AuNBPs, as shown in Figure S1 (Supporting Information). It was found that when using 8 mM NaOL for AuNBP synthesis, the lowest CTAB concentration that could be achieved was 50 mM; concentrations lower than this did not yield AuNBPs. Therefore, we opted to fix the CTAB concentration at 40 mM and adjusted the NaOL concentration within the range of 0–9 mM, as illustrated in Figure S2 (Supporting Information). We observed that NaOL concentrations between 2–6 mM enabled AuNBP synthesis, which was lower compared to the previously used 8 mM concentration.

Based on the above results, we further reduced the CTAB concentration and made minor adjustments to the NaOL concentration. As shown in Figure S3 (Supporting Information), when the CTAB concentration was 30 mM, AuNBPs could be synthesized with NaOL concentrations ranging from 2–4 mM, indicating a narrower range and lower concentration compared to previous conditions. In Figure S4 (Supporting Information), with a CTAB concentration of 20 mM, NaOL concentrations needed to be within 1–2 mM to synthesize AuNBPs. Figures S5 and S6 (Supporting Information) demonstrated that at a CTAB concentration of 10 mM, AuNBPs could only be synthesized with NaOL concentrations ≈2 mM. Decreasing NaOL concentration led to a decrease in spectral intensity and a slight blue shift in peak position while increasing NaOL concentration resulted in a rapid decrease in spectral intensity and a significant red shift in peak position.

Based on these findings, we attempted to further reduce the CTAB concentration. However, experiments with 9 mM CTAB, as shown in Figure S7 (Supporting Information), did not yield AuNBPs with suitable NaOL concentrations within the 1–2 mM. To mitigate possible errors, we continued experiments with 8 mM CTAB, as depicted in Figure S8 (Supporting Information), which similarly did not yield suitable concentrations of AuNBPs within the 1–2 mM NaOL range.

Additionally, we compared the data for synthesizing AuNBPs using a single surfactant, CTAB, with reduced CTAB concentrations. As shown in Figure S9 (Supporting Information), this figure presents the spectra of AuNBPs synthesized with varying CTAB concentrations when the NaOL concentration is 0. The spectra indicate that under otherwise unchanged conditions, AuNBPs could not be synthesized with CTAB concentrations ranging from 40 to 10 mM.

Therefore, based on these experimental results, we conclude that the minimum effective surfactant concentrations for synthesizing AuNBPs using the dual-surfactant method described in this study are 10 of CTAB and 2 mM of NaOL. The CTAB concentration cannot be further reduced, and the range of NaOL concentration varies with increasing CTAB concentration, higher CTAB concentrations widen the acceptable range of NaOL concentrations. Although further reduction of CTAB concentration in our experiments may not be practical, our synthesis method is not exclusively applicable to the synthesis of AuNBPs. In fact, the dual surfactant approach using CTAB and NaOL has been employed for the synthesis of AuNRs as well. Therefore, we believe that this dual surfactant method can be equally effective for the growth of other nanoparticles synthesized through seed-mediated growth methods. Although the AuNBPs synthesized in our study have not undergone actual biological testing, we have indeed succeeded in reducing the CTAB concentration. While additional purification and cleaning would still be required for biomedical applications, our approach offers a potential synthesis pathway that could be suitable for such applications.

To further verify the influence of the morphology and size of AuNBPs on their spectra, we conducted FDTD simulations to calculate the full-field scattering spectra and electric field distributions of AuNBPs with different sizes.

In the FDTD simulations, we first modeled the AuNBPs based on the experimentally obtained sizes by changing the seed volume. As shown in Figure S10 (Supporting Information), we used the built-in conical shape model in the FDTD software to create two back-to-back cones. Detailed cone data can be found in Table S1 (Supporting Information), resulting in the AuNBP model we needed. Then, we set up a total-field scattered-field light source, where the polarization direction of the light source is parallel to the long axis of the AuNBP, and the propagation direction is perpendicular to the long axis of the AuNBP, with a wavelength range of 300–1100 nm.

Figure 5 shows the full-field scattering spectra obtained from the FDTD simulations, along with the corresponding LSPR peak positions and intensity changes. Figure S11a (Supporting Information) shows the raw data of the full-field scattering spectrum from the FDTD simulations, while Figure S11b (Supporting Information) shows the corresponding normalized data.

From Figure S11a,b (Supporting Information), one can observe that the LSPR peak position in the simulated spectra of AuNBPs gradually redshifts with the increase in the size of the AuNBP model, and the intensity gradually increases. The LSPR peak positions in the simulation results highly coincide with those in the experimental results, but the LSPR peak intensity differs due to the varying gold concentrations, showing no consistency with the experimental results. Therefore, we measured the sizes of different AuNBPs from Table S1 (Supporting Information) and calculated their respective volumes. Then, based on the volume of the largest AuNBP, we calculated the volume ratios of smaller AuNBPs to it. This ratio can be reasonably assumed to represent the difference in the number of AuNBPs in solutions synthesized using different seed volumes. The above data can be found in Table S4 (Supporting Information). We then multiplied the corresponding spectra in Figure S11a (Supporting Information) by these ratios to obtain the image in Figure 5.

As shown in Figure 5, the LSPR peak intensity in the simulated results also shows a trend of first increasing and then decreasing, similar to the experimental results. The LSPR peak intensities in the simulation reach their maximum when the seed volume is 200 µL, whereas in the experiment, the highest is at 50–100 µL. We believe this discrepancy is due to the increase in impurities as the seed volume increases, which relatively weakens the LSPR peak intensity in the experimental synthesis of AuNBPs. In contrast, the simulation only calculates the number of AuNBPs based on their volume, leading to some differences.

Figure S10 (Supporting Information) shows the electric field intensity distribution from the FDTD simulations. When the AuNBP is excited along the long axis, the enhancement of the electric field is mainly localized at the two tips of the AuNBP. The

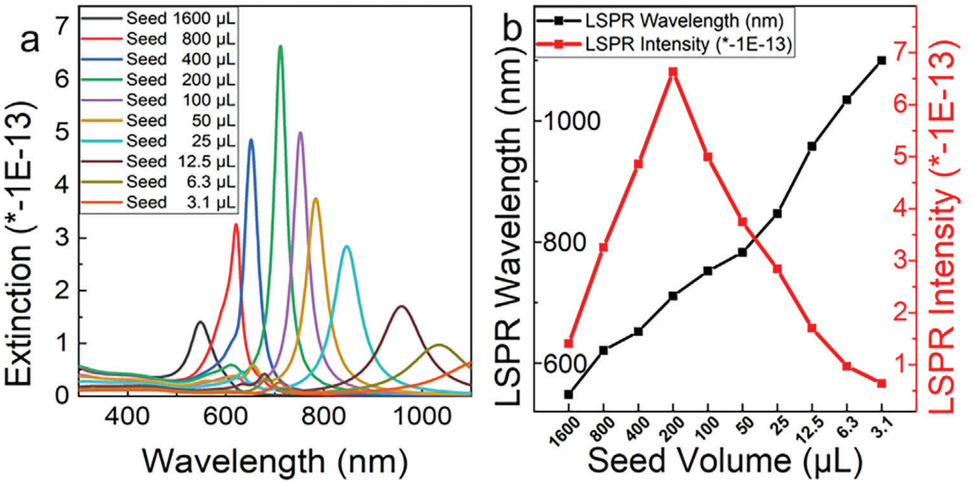

Figure 5. The full-field scattering spectra a) and corresponding LSPR peak positions and intensities b) of AuNBPs with different sizes were obtained from FDTD simulations after intensity corrections.

intensities also increase first and then decrease with the increase of the AuNBP size, which is consistent with the experimental results.

3. Conclusion

In summary, we have conducted a series of experiments by introducing NaOL in the synthesis of AuNBPs and reduced the CTAB concentration to 10 mM. During the experiments, we successfully controlled the size and morphology of the synthesized AuNBPs by varying the seed solution volume, achieving sizes ranging from ≈20 in length and 13 nm in width to ≈280 in length and 70 nm in width. By controlling the Ag^+ ion content, we have identified the optimal concentration for synthesizing AuNBPs, with the corresponding amount of $AgNO_3$ being 50 µL. We also investigated the causes of abnormal white precipitate formation and proposed solutions. Additionally, by adjusting the solution pH, we identified the optimal pH for AuNBP synthesis, with the corresponding amount of HCl being 1600 µL; excessively high pH values led to too rapid reduction rates, disrupting selective deposition of gold on the seed surface, preventing AuNBP formation, while too low pH values resulted in very slow reaction rates and prolonged experimental times. FDTD simulations also confirmed the spectral modulation of AuNBP sizes. Based on these results, we demonstrated the feasibility of the NaOL modification method in reducing CTAB concentration and successfully synthesized a range of AuNBPs of different sizes while maintaining the high monodispersity of the final product. This method can serve as a template for further practical applications and provide improved schemes for other nanoparticle synthesis.

4. Experimental Section

Materials: All chemicals were obtained from commercial suppliers and used without further purification. Cetyltrimethylammonium chloride (CTAC, 99%), hexadecyltrimethylammonium bromide (CTAB, 99%), l-ascorbic acid (AA, 99.99%) were purchased from Shanghai Macklin Biochemical Technology Co., Ltd. Sodium citrate tribasic dehydrate (SC, 99%), gold III chloride trihydrate ($HAuCl_4$, AR), sodium borohydride ($NaBH_4$, 98%), sodium oleate (NaOL, CP), silver nitrate ($AgNO_3$, 99.99%), hydrochloric acid (HCl, 37 wt.% in water, 12.1 mM), benzyldimethylhexadecylammonium chloride (HDBAC, 95%) were purchased from Shanghai Aladdin Biochemical Technology Co., Ltd. Ultrapure water (Millipore Milli-Q grade) with a resistivity of 18.2 MΩ was used in all of the experiments.

Synthesis of Gold Nanobipyramids—Preparation of Seed Solution: 5 mL of 0.1 mM CTAC solution, 5 mL of 0.01 mM SC solution, and 0.25 mL of 0.01 mM $HAuCl_4$ solution were mixed in a scintillation vial. A magnetic stir bar was added and, while stirring vigorously at 1200 rpm, added 0.25 mL of 0.025 mM $NaBH_4$ solution freshly prepared by ice water. Stirring was continued for 1 min. The prepared solution was transfered to a water bath set at 80 °C and let it stand for 90 min. The solution would change color from brownish-yellow to red. Finally, the seed solution was removed from the water bath and stored at room temperature.

The specific synthesis parameters can be referenced in Table S5a (Supporting Information).

Synthesis of Gold Nanobipyramids—Preparation of AuNBPs: The following synthesis process details a specific method, with other methods differing only slightly in the volume and concentration of the reagents used, while the experimental steps remain fundamentally the same.

20 mL of 0.01 mM CTAB solution, 200 µL of 0.2 mM NaOL solution was mixed, and 1 mL of 0.01 mM $HAuCl_4$ solution in a scintillation vial. A magnetic stir bar was added and the vial was placed in a 30 °C water bath. It was slowly Stirred at 150 rpm for over 60 min, ensuring the solution changes color from yellow to colorless and transparent. While stirring at 150 rpm, sequentially added 50 µL of 0.01 mM $AgNO_3$ solution, 1600 µL of 1 mM HCl aqueous solution, 50 µL of 0.1 mM AA solution, and 50 µL of the seed solution, ensuring thorough mixing after each addition. Then, the solution was placed in a 30 °C water bath and stir slowly at 150 rpm for 24 h to allow complete growth of the AuNBPs.

The specific synthesis parameters can be referenced in Table S5b (Supporting Information) with modifications as indicated in Tables S1–S3 (Supporting Information).

Purification of AuNBPs: The following purification process details a specific method, with other methods differing slightly in conditions.

To purify AuNBPs, centrifuge the solution at 8000 rpm for 10 min. Supernatant was removed and the precipitate was redispersed in 7.2 mL of 1.5 mM CTAB solution in a scintillation vial. Then, 12.8 mL of 0.5 mM HDBAC solution was added. The solution was placed in a 30 °C water bath and let it stand for 12 h. The AuNBP particles will flocculate and settle at the bottom of the vial, while smaller spherical impurities will remain in the supernatant. Carefully remove the pink supernatant, then redisperse the precipitate in 5 mL of 1.5 mM CTAB solution. The resulting brown purified solution was centrifuged at 8000 rpm for 10 min and washed with 5 mL of 1.5 mM CTAB solution to remove excess HDBAC. Finally, the purified AuNBPs were dispersed in 1.0 mL of 1.5 mM CTAB solution, making them ready for further experimental studies.

Characterization: Optical extinction spectra were recorded with a UV-1900i Spectrophotometer (Shimadzu, Japan) with a 10 mm optical path. Transmission electron microscopy (TEM) images were obtained with an HT-7700 microscope (Hitachi, Japan) operating at 100 kV. The particle sizes of the AuNBPs were measured from TEM images, whereby >50 particles were measured for each sample.

Supporting Information

Supporting Information is available from the Wiley Online Library or from the author.

Acknowledgements

The authors thank Sudan Shen for her assistance in TEM at the State Key Laboratory of Chemical Engineering (Zhejiang University). T.S. Deng acknowledges financial support from Zhejiang Provincial Natural Science Foundation (Grant: LY24F050008), Zhejiang Provincial Educational Ministry Scientific Research Project (Grant: Y202352284), and National Natural Science Foundation of China (NSFC, Grant: 61905056). This work was also supported by the Fundamental Research Funds for the Provincial Universities of Zhejiang (GK239909299001-301).

Conflict of Interest

The authors declare no conflict of interest.

Data Availability Statement

The data that support the findings of this study are available in the supplementary material of this article.

Keywords

gold nanobipyramids, hexadecyltrimethylammonium bromide, localized surface plasmon resonance, seed-mediated synthesis, sodium oleate

Received: August 9, 2024
Revised: August 22, 2024
Published online:

---

[1] K. A. Dahan, Y. Li, J. Xu, C. X. Kan, *Phys. Chem. Chem. Phys.* **2023**, *25*, 18545.
[2] J. Cao, T. Sun, K. T. V. Grattan, *Sens. Actuator B-Chem.* **2014**, *195*, 332.
[3] B. Wu, D. Liu, S. Mubeen, T. T. Chuong, M. Moskovits, G. D. Stucky, *J. Am. Chem. Soc.* **2016**, *138*, 1114.
[4] X. Zhu, H. Jia, X. M. Zhu, S. Cheng, X. Zhuo, F. Qin, Z. Yang, J. Wang, *Adv. Funct. Mater.* **2017**, *27*, 1700016.
[5] F. X. Xiao, B. Liu, *Adv. Mater. Interfaces* **2018**, *5*, 1701098.
[6] S. Linic, P. Christopher, D. B. Ingram, *Nat. Mater.* **2011**, *10*, 911.
[7] Q. Li, X. L. Zhuo, S. Li, Q. F. Ruan, Q. H. Xu, J. F. Wang, *Adv. Opt. Mater.* **2015**, *3*, 801.
[8] Q. Shi, K. J. Si, D. Sikdar, L. W. Yap, M. Premaratne, W. Cheng, *ACS Nano* **2016**, *10*, 967.
[9] S. Yougbare, H. L. Chou, C. H. Yang, D. I. Krisnawati, A. Jazidie, M. Nuh, T. R. Kuo, *J. Hazard. Mater.* **2021**, *407*, 124617.
[10] A. Yusuf, A. R. Z. Almotairy, H. Henidi, O. Y. Alshehri, M. S. Aldughaim, *Polymers* **2023**, *15*, 1596.
[11] T. H. Chow, N. N. Li, X. P. Bai, X. L. Zhuo, L. Shao, J. F. Wang, *Accounts Chem. Res.* **2019**, *52*, 2136.
[12] D. Chateau, A. Desert, F. Lerouge, G. Landaburu, S. Santucci, S. Parola, *ACS Appl. Mater. Interfaces* **2019**, *11*, 39068.
[13] J. L. Lv, X. H. Sun, Q. Q. Zhan, S. L. He, E. Forsberg, *Mater. Res. Express* **2020**, *7*, 025029.
[14] X. Ye, C. Zheng, J. Chen, Y. Gao, C. B. Murray, *Nano Lett.* **2013**, *13*, 765.
[15] X. Zhang, N. Tran, T. Egan, B. Sharma, G. Chen, *J. Phys. Chem. C* **2021**, *125*, 13350.
[16] Y. Ni, C. X. Kan, J. Xu, *Phys. Chem. Chem. Phys.* **2022**, *24*, 21522.
[17] J. H. Lee, K. J. Gibson, G. Chen, Y. Weizmann, *Nat. Commun.* **2015**, *6*, 7571.
[18] A. Sanchez-Iglesias, N. Winckelmans, T. Altantzis, S. Bals, M. Grzelczak, L. M. Liz-Marzan, *J. Am. Chem. Soc.* **2017**, *139*, 107.
[19] M. Z. Liu, P. Guyot-Sionnest, *J. Phys. Chem. B* **2005**, *109*, 22192.
[20] X. L. Liang, Y. L. Yang, C. Zou, W. Chen, H. X. Zou, Y. Yang, *Colloid Surf. A-Physicochem. Eng. Asp.* **2020**, *597*, 124749.
[21] G. González-Rubio, L. Scarabelli, A. Guerrero-Martínez, L. M. Liz-Marzán, *ChemNanoMat* **2020**, *6*, 698.
[22] X. Zhang, R. Gallagher, D. He, G. Chen, *Chem. Mat.* **2020**, *32*, 5626.
[23] T. Zhang, X. Li, Y. Sun, D. Liu, C. Li, W. Cai, Y. Li, *Chem. Sci.* **2021**, *12*, 12631.
[24] Q. Zhong, J. Feng, B. Jiang, Y. Fan, Q. Zhang, J. Chen, Y. Yin, *J. Am. Chem. Soc.* **2021**, *143*, 20513.
[25] J. Chen, Y. Bai, J. Feng, F. Yang, P. Xu, Z. Wang, Q. Zhang, Y. Yin, *Angew. Chem.-Int. Edit.* **2021**, *60*, 4117.
[26] S. Wang, W. Lu, O. Tovmachenko, U. S. Rai, H. Yu, P. C. Ray, *Chem. Phys. Lett.* **2008**, *463*, 145.
[27] I. P. Lau, H. Chen, J. Wang, H. C. Ong, K. C. F. Leung, H. P. Ho, S. K. Kong, *Nanotoxicology* **2012**, *6*, 847.
[28] A. Rajeshwari, B. Roy, N. Chandrasekaran, A. Mukherjee, *Plant Physiol. Biochem.* **2016**, *109*, 209.
[29] J. He, S. Unser, I. Bruzas, R. Cary, Z. Shi, R. Mehra, K. Aron, L. Sagle, *Colloid Surf. B-Biointerfaces* **2018**, *163*, 140.
[30] A. P. Leonov, J. Zheng, J. D. Clogston, S. T. Stern, A. K. Patri, A. Wei, *ACS Nano* **2008**, *2*, 2481.

Supporting Information

Seed-Mediated Synthesis of Gold Nanobipyramids at Low CTAB Concentration Using Binary Surfactants

Er-Ji Zhang[1], Tian-Song Deng[1,*], Zhuo Chen[1], Li-Yong Liu[1], Gui-LinWu[1], Yu-Chun Cheng[1], Jia-Fei Gao[1], Kun-Peng Wang[1], and Jie Liu[1]

[1]*School of Electronics and Information Engineering, Hangzhou Dianzi University, Hangzhou 310018, P. R. China*

* *Corresponding author. E-mail: dengts@pku.edu.cn*

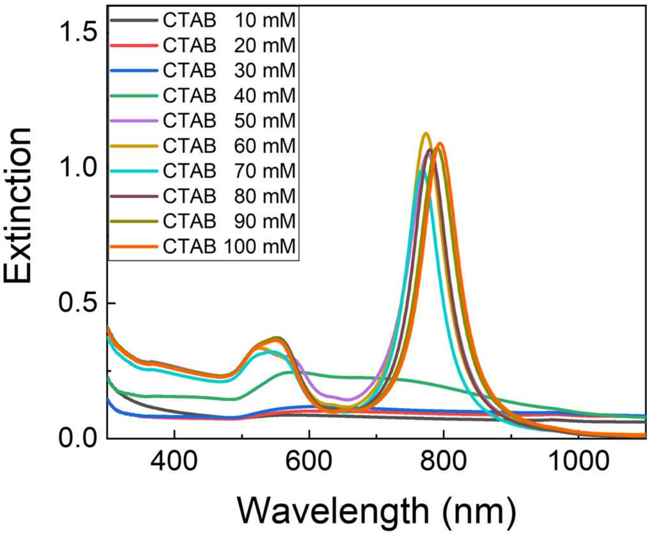

Figure S1. UV-vis-NIR spectra of AuNBPs synthesized by adjusting the CTAB concentration within the range of 10-100 mM at a NaOL concentration of 8 mM.

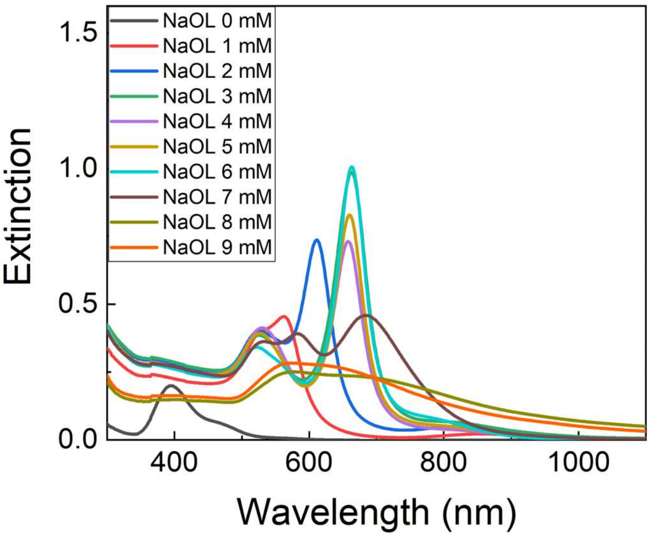

Figure S2. UV-vis-NIR spectra of AuNBPs synthesized by adjusting the NaOL concentration within the range of 0-9 mM at a CTAB concentration of 40 mM.

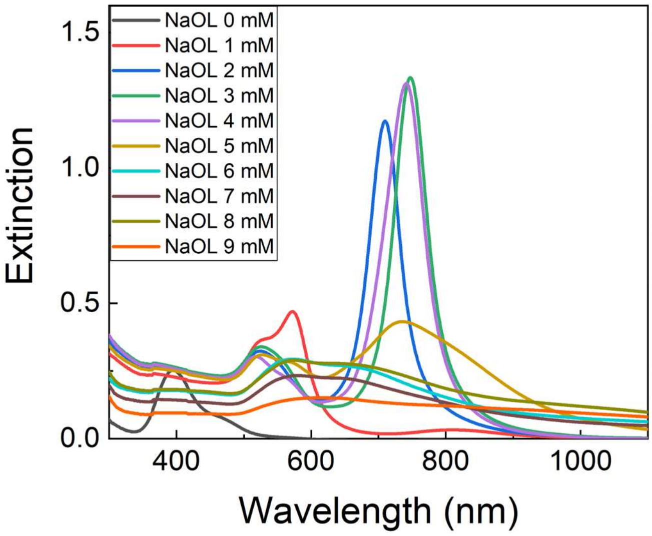

Figure S3. UV-vis-NIR spectra of AuNBPs synthesized by adjusting the NaOL concentration within the range of 0-9 mM at a CTAB concentration of 30 mM.

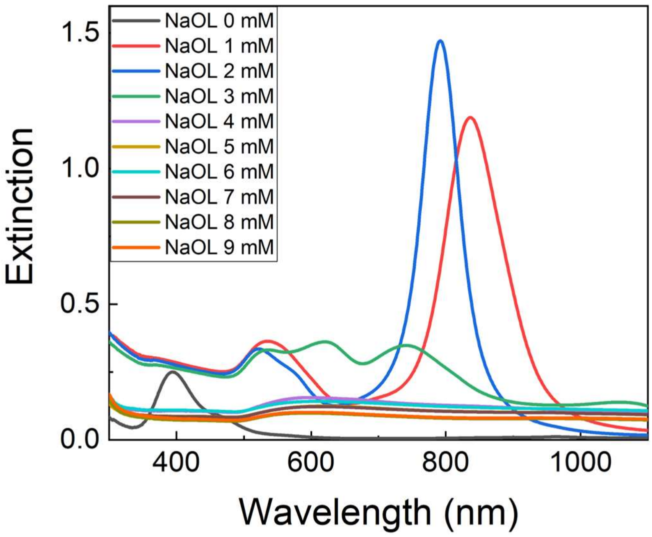

Figure S4. UV-vis-NIR spectra of AuNBPs synthesized by adjusting the NaOL concentration within the range of 0-9 mM at a CTAB concentration of 20 mM.

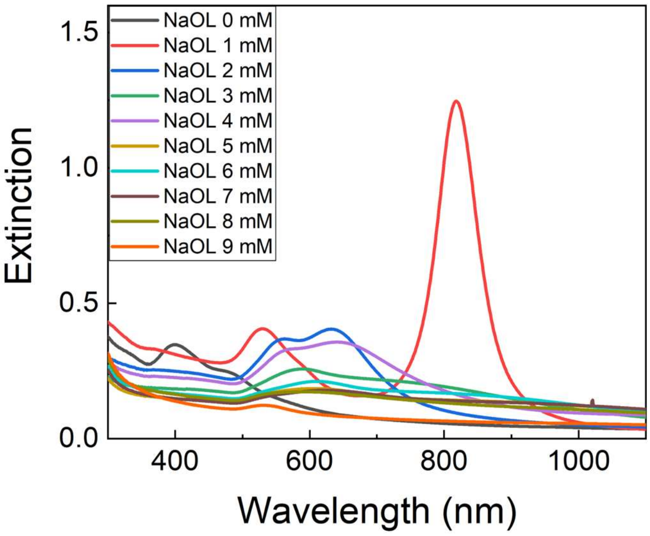

Figure S5. UV-vis-NIR spectra of AuNBPs synthesized by adjusting the NaOL concentration within the range of 0-9 mM at a CTAB concentration of 10 mM.

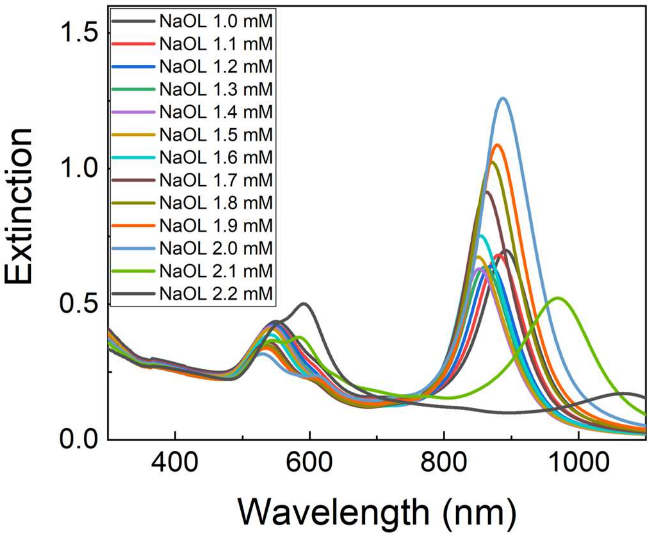

Figure S6. UV-vis-NIR spectra of AuNBPs synthesized by adjusting the NaOL concentration within the range of 1.0-2.2 mM at a CTAB concentration of 10 mM.

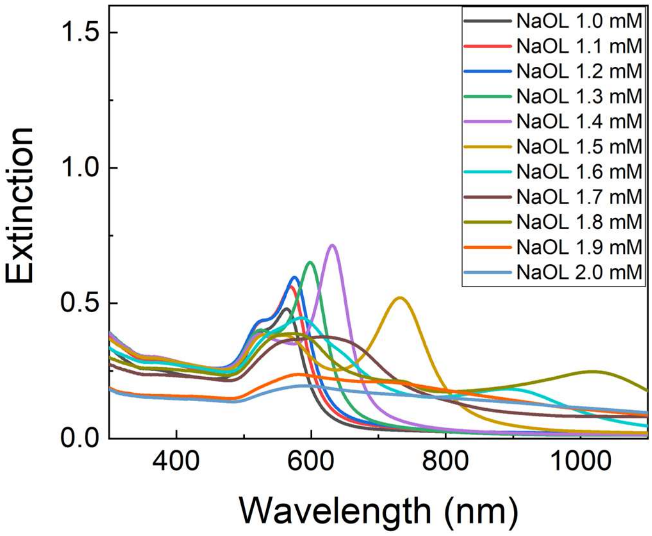

Figure S7. UV-vis-NIR spectra of AuNBPs synthesized by adjusting the NaOL concentration within the range of 1.0-2.0 mM at a CTAB concentration of 9 mM.

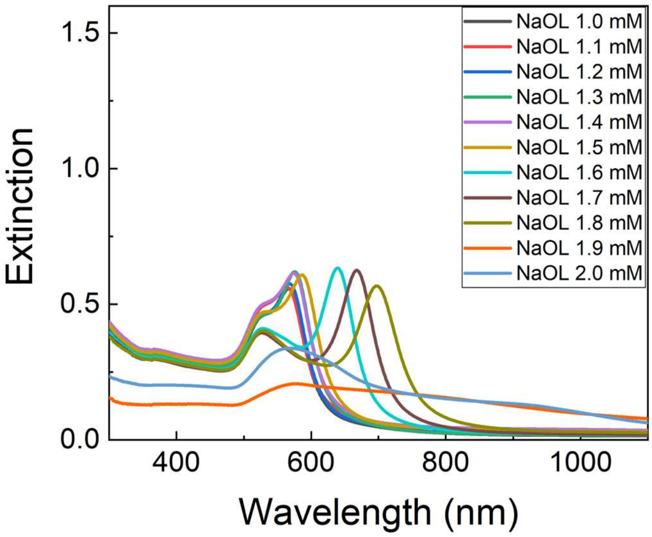

Figure S8. UV-vis-NIR spectra of AuNBPs synthesized by adjusting the NaOL concentration within the range of 1.0-2.0 mM at a CTAB concentration of 8 mM.

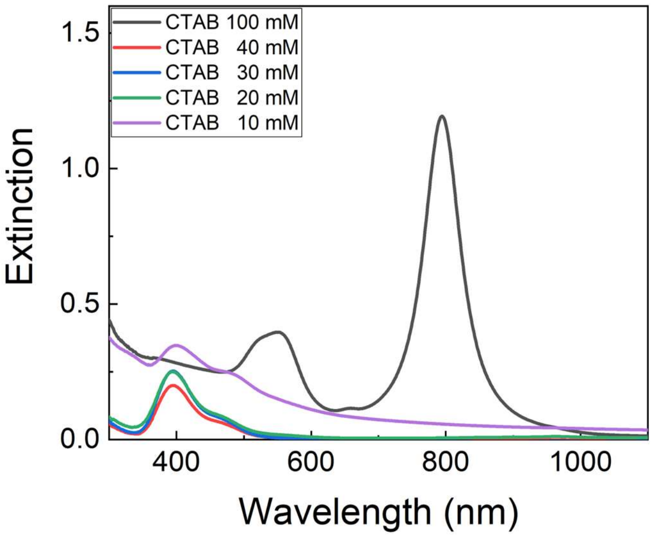

Figure S9. UV-vis-NIR spectra of AuNBPs synthesized by adjusting the CTAB concentration within the range of 10-100 mM at the NaOL concentration of 0.

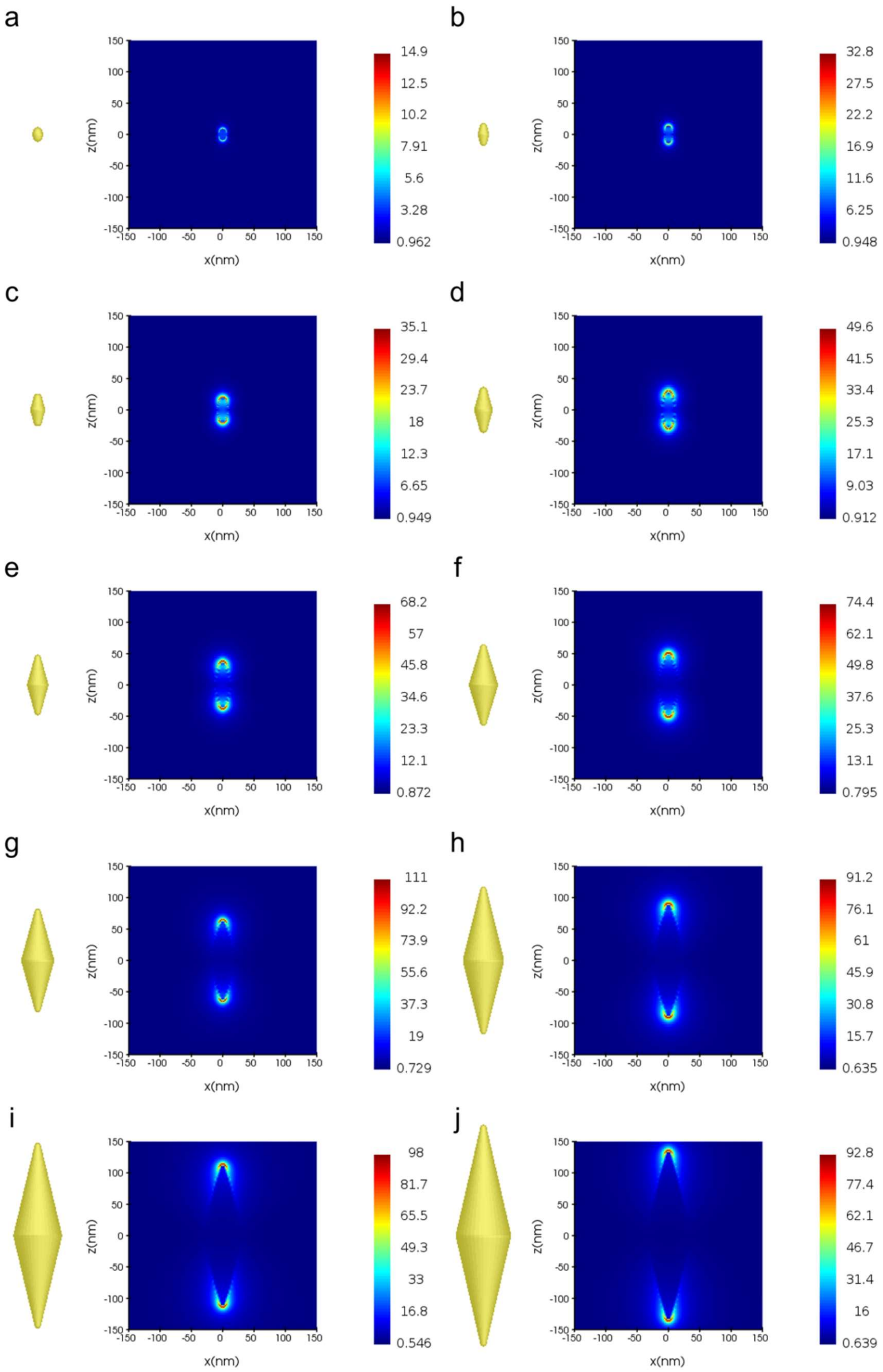

Figure S10. The electric field intensity distribution image of AuNBPs of different sizes obtained from FDTD simulations, the maximum electric field strengths from a to i are 14.9, 32.8, 35.1, 49.6, 68.2, 74.4, 111, 91.2, 98, and 92.8.

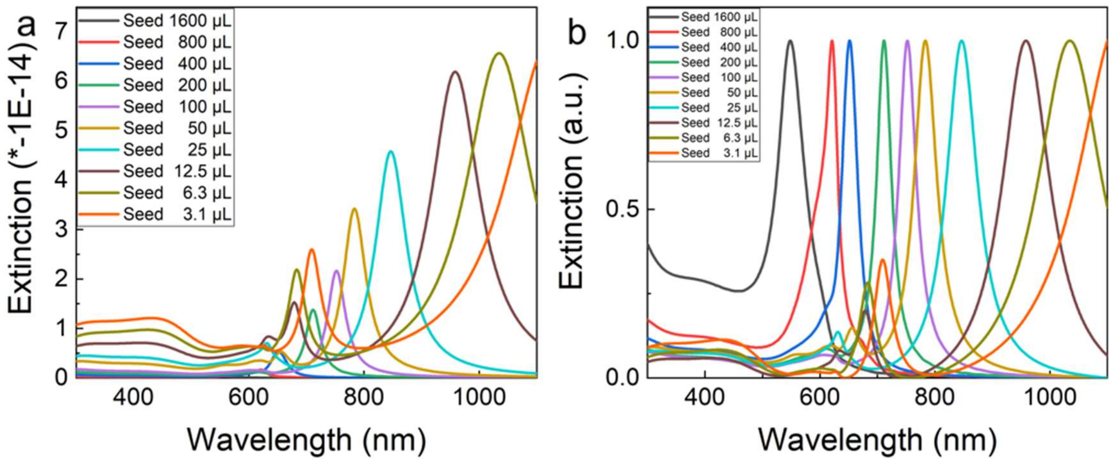

Figure S11. The original (a) and normalized (b) of the full-field scattering spectra of AuNBPs of different sizes obtained from FDTD simulations.

Table S1. The LSPR peak positions, lengths and widths of AuNBPs synthesized with different seed volumes.

Seed Volume (μL)	LSPR Wavelength (nm)	Length (nm)	Width (nm)
1600	531	18.3±0.7	13.1±0.5
800	616	28.5±1.7	14.7±0.8
400	655	40.6±1.7	18.0±0.9
200	710	56.3±2.8	21.0±1.0
100	748	74.5±3.2	26.4±1.0
50	788	100.5±4.1	33.0±1.2
25	841	126.4±4.4	39.1±1.8
12.5	944	180.8±5.4	49.1±2.7
6.3	1026	226.6±9.6	59.8±3.3
3.1	1100	269.5±8.1	66.7±4.1

Table S2. The LSPR peak positions of AuNBPs synthesized with different $AgNO_3$ volumes.

$AgNO_3$ Volume (μL)	LSPR Wavelength (nm)
0	531
25	837
50	863
100	874
200	895
400	897
800	896
1600	891
3200	899
6400	883

Table S3. The LSPR peak positions of AuNBPs synthesized with different HCl volumes.

HCl Volume (μL)	LSPR Wavelength (nm)
0	534
100	973
200	942
400	895
800	868
1600	873
3200	850
4800	841
6400	831
8000	822

Table S4. The volumes and relative quantity multiples of AuNBPs calculated from raw data from Table S1.

Seed Volume (μL)	AuNBP Volume (nm^3)	Relative Multiple
1600	821.8	381.8
800	1611.5	194.7
400	3442.1	91.2
200	6496.7	48.3
100	13586.7	23.1
50	28638.0	11.0
25	50564.9	6.2
12.5	114053.8	2.8
6.3	212036.5	1.5
3.1	313732.0	1.0

Table S5. The specific parameters used for synthesizing AuNBPs.

(a) Seed Solution:

Reagents	Concentration	Volume
CTAC	0.1 M	5 mL
SC	0.01 M	5 mL
$HAuCl_4$	0.01 M	0.25 mL
$NaBH_4$	0.025 M	0.25 mL

(b) Growth Solution:

Reagents	Concentration	Volume
CTAB	0.1 M	20 mL
NaOL	0.2 M	0.2 mL
$HAuCl_4$	0.01 M	1 mL
$AgNO_3$	0.01 M	50 μL
HCl	12.1 M	132 μL
AA	0.1 M	50 μL
Seed Solution	--	50 μL